

Modeling of a dual-capacitor neuron without an inductor

Zhen-Hua Yu(于振华), Yu-Chen Zhang(张钰晨), and Fei-Fei Yang(杨飞飞)
Citation: Chin. Phys. B, 2026, 35 (**6**): 060513. DOI: 10.1088/1674-1056/ae77d3
http://cpb.iphy.ac.cn; http://iopscience.iop.org/cpb

What follows is a list of articles you may be interested in

Synchronization of neuromorphic memristive Josephson junction network and its application

Dejun Yan(严德军), Fuqiang Wu(吴富强), and Wenshuai Wang(汪文帅)
Chin. Phys. B, 2026, 35 (**1**): 010505. DOI: 10.1088/1674-1056/ae1456

Dynamical behaviors of a multifunctional neural circuit

Xiao-Hong Gao(高晓红), Kai-Long Zhu(朱凯龙), and Fei-Fei Yang(杨飞飞)
Chin. Phys. B, 2025, 34 (**9**): 090503. DOI: 10.1088/1674-1056/ae001b

A novel non-autonomous hyperchaotic map based on discrete memristor parallel connection

Weiping Wu(吴伟平), Mengjiao Wang(王梦蛟), and Qigui Yang(杨启贵)
Chin. Phys. B, 2025, 34 (**5**): 050503. DOI: 10.1088/1674-1056/adb8bc

Dynamics and synchronization of neural models with memristive membranes under energy coupling

Jingyue Wan(万婧玥), Fuqiang Wu(吴富强), Jun Ma(马军), and Wenshuai Wang(汪文帅)
Chin. Phys. B, 2024, 33 (**5**): 050504. DOI: 10.1088/1674-1056/ad1dcc

Firing activities in a fractional-order Hindmarsh-Rose neuron with multistable memristor as autapse

Zhi-Jun Li(李志军), Wen-Qiang Xie(谢文强), Jin-Fang Zeng(曾金芳), and Yi-Cheng Zeng(曾以成)
Chin. Phys. B, 2023, 32 (**1**): 010503. DOI: 10.1088/1674-1056/ac65f7

SPECIAL TOPIC — Biophysical circuits: Modeling & applications in neuroscience

Modeling of a dual-capacitor neuron without an inductor

Zhen-Hua Yu(于振华), Yu-Chen Zhang(张钰晨), and Fei-Fei Yang(杨飞飞)†

College of Artificial Intelligence and Computer Science, Xi'an University of Science and Technology, Xi'an 710054, *China*

(Received 23 April 2026; revised manuscript received 2 June 2026; accepted manuscript online 4 June 2026)

The physical circuit model of biological neurons can be obtained by applying electronic components to simulate the ion channels and membrane potential of biological neurons. The effective physical circuit model of neurons provides an experimentally verifiable physical carrier for understanding the information encoding mechanism of the nervous system. In addition, the nonlinear dynamic characteristics of the physical circuit model of the neuron lay the bionic foundation for brain-inspired computing and the design of low-power neuromorphic chips. Therefore, this paper designs a dual-capacitor memristive neural circuit without any inductive elements and analyzes the nonlinear dynamic characteristics of the physical circuit model of the neuron. First, Kirchhoff's current law is applied to derive the differential equations describing the memristive neural circuit, and a neural dynamics model expressed by the differential equations is established. The corresponding energy function of the memristive neural circuit is derived based on Helmholtz's theorem. Subsequently, nonlinear dynamical analysis methods are employed to investigate the complex dynamical behaviors of this neural model. The results indicate that the electrical activity of the neuron can be effectively modulated by external stimuli and external magnetic fields; specifically, this neuron model exhibits stochastic resonance phenomena under a noisy magnetic field. Furthermore, the neuron's self-regulatory capability is verified using an adaptive method based on energy ratio control. The hardware feasibility of this neuronal model is further validated through LTspice simulation. Finally, this neuronal model can be coupled to form a neural network for investigating the collective behaviors of neural networks and the influence of external magnetic fields on their collective properties.

Keywords: memristive neuron, dynamical behaviors, LTspice simulation

PACS: 05.45.–a

DOI: 10.1088/1674-1056/ae77d3 **CSTR:** 32038.14.CPB.ae77d3

1. Introduction

Memristors are the fourth fundamental type of electronic component. Chua[1] first predicted the theory of the memristor in 1971. A memristor was physically realized by the Hewlett–Packard Laboratories not until 2008.[2] Due to the memristor's inherent non-linearity and memory properties, they are widely used in non-linear circuits, chaotic circuits, chaotic systems, neurons and neural networks.

Adding a memristor to a nonlinear circuit yields a memristor chaotic circuit, such as simple memristor chaotic circuits,[3–5] magnetic flux-controlled memristive chaotic circuits,[6,7] charge-controlled memristive chaotic circuits,[8] and voltage-controlled memristive chaotic circuits.[9] Introducing a memristor into a chaotic system can generate a memristor chaotic system; these systems exhibit various complex dynamical behaviors, such as multi-stability,[9,10] hidden attractors,[11,12] and coexisting attractors.[13–15] Memristor chaotic systems are physically verified with analog circuits[16–18] and digital circuits.[19–21] Moreover, adding a discrete memristor to a chaotic map leads to memristor chaotic maps.[22–24] Many chaotic maps[25–28] are built based on memristor coupled circuits. Recent research suggests that general chaotic mappings can also be represented by memristor circuits.[29]

External stimuli are known to play an important role in regulating neuronal dynamics. Previous studies have reported chaotic resonance and firing-pattern transitions in type-I and type-II Morris–Lecar neurons, astrocyte-coupled neurons, and Hodgkin–Huxley neurons under external stimulation.[30–32] These findings suggest that external inputs can effectively modulate neuronal firing activities and enrich the dynamical behaviors of neuron models. Recently, memristors are widely researched in neuron models and neural networks. Many memristive neuron models are obtained by introducing a memristor into a neuron model, such as memristive HR neuron models,[33,34] and memristive FHN neuron models.[35,36] Many memristive neuron models are built based on memristor circuits, for example, magnetic flux-controlled memristive neuron models,[37,38] charge-controlled neuron models,[39] dual-memristor neuron models,[40,41] memristive membrane neuron models,[42–44] and memristor ion channel neuron models.[45–47]

While extensive efforts have been devoted to developing memristive neuron models, memristive neural networks have also attracted increasing attention in recent years. Synchronization, chimera states, and learning behaviors have been reported in memristor-coupled neuronal networks, highlighting the potential of memristive devices for large-scale neuro-

†Corresponding author. E-mail: dlpuyff@sina.com, yangfeifei@xust.edu.cn

© 2026 Chinese Physical Society and IOP Publishing Ltd. All rights, including for text and data mining, AI training, and similar technologies, are reserved.

morphic computing applications.[48,49] The existing memristor neuron models: some focus solely on the functional aspects of biological neurons,[50,51] some on their biological structure, and others on the regulation of neuronal electrical activity by external electromagnetic fields; none, however, address the challenge of integrating large numbers of memristor neuron models. Consequently, this paper designs a dual-capacitor memristor neuron model without inductor based on the structure of biological neurons and considerations of ease of integration.

The main contributions of this work are given as follows: (1) A dual capacitor memristive neural circuit without an inductor is designed for ease of integration. (2) The neuronal firing behaviors under external stimulus and magnetic fields are revealed. (3) An energy-based adaptive scheme is proposed to effectively regulate neuronal firing patterns.

This paper is structured as follows: Section 2 establishes the dual-capacitor memristive neuron model. Section 3 analyzes the neuron's dynamical behaviors under external stimuli and electromagnetic fields. Section 4 summarizes the main results.

2. Model and scheme

From the viewpoint of physics, a biological neuron can be modeled based on a nonlinear circuit constructed with physical electronic components. Different nonlinear circuits constructed from various electronic components can describe the characteristics of different biological neurons. This paper designs a dual-capacitor neural circuit without an inductor; the corresponding schematic circuit diagram is displayed in Fig. 1.

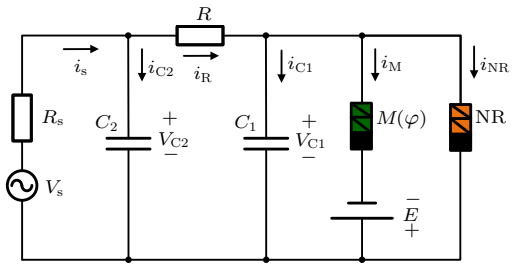


Fig. 1. A neural circuit with two capacitors.

The neural circuit in Fig. 1 is composed of eight electronic components. It contains two capacitors (C_1, C_2), two linear resistors (R_s, R), two voltage sources (V_s, E), a memristor ($M(\varphi)$), and a nonlinear resistor (NR). The linear resistor (R) is connected in parallel with two capacitors (C_1, C_2) and represents the double-membrane structure of a biological neuron. A memristor ($M(\varphi)$) is connected in series with a feedback voltage (E) to simulate the ion channels of a neuron. A nonlinear resistor (NR) is used to describe the nonlinear characteristics of the electric field and magnetic field generated during ion transport. The voltage source (V_s) drives this neural circuit by simulating external stimuli.

The memristor in the fourth branch of the neural circuit in Fig. 1 is defined as follows:

$$\begin{cases} i_M = \alpha M(\varphi) V_M = \alpha \varphi V_M, \\ \dfrac{d\varphi}{dt} = -\lambda\varphi + \delta V_M, \end{cases} \tag{1}$$

where (δ, α, λ) denote the parameters of the material. (i_M, V_M, φ) denote the current, voltage, and magnetic flux through the memristor branch. The nonlinear resistor[35] in the fifth branch of the neural circuit in Fig. 1 is described by

$$i_{NR} = -\frac{1}{\rho}\left(V - \frac{V^3}{3V_0^2}\right), \tag{2}$$

where ρ is the resistance, (i_{NR}, V) denote the current and voltage through the nonlinear resistor branch, and V_0 is the cut-off voltage of the nonlinear resistor. In this paper, V is equivalent to V_{C1}. Applying Kirchhoff's laws to the neural circuit shown in Fig. 1 yields the following branch current relationship:

$$\begin{cases} i_{C1} = i_R - i_M - i_{NR}, \\ i_{C2} = i_s - i_R. \end{cases} \tag{3}$$

Equation (3) can be further updated as follows:

$$\begin{cases} C_1 \dfrac{dV_{C1}}{dt} = \dfrac{(V_{C2} - V_{C1})}{R} - \alpha\varphi(V_{C1} + E) \\ \qquad\qquad + \dfrac{1}{\rho}\left(V_{C1} - \dfrac{V_{C1}^3}{3V_0^2}\right), \\ C_2 \dfrac{dV_{C2}}{dt} = \dfrac{(V_s - V_{C2})}{R_s} - \dfrac{(V_{C2} - V_{C1})}{R}, \\ \dfrac{d\varphi}{dt} = -\lambda\varphi + \delta(V_{C1} + E). \end{cases} \tag{4}$$

The variables in Eq. (4) are redefined by

$$x = \frac{V_{C1}}{V_0}, \quad y = \frac{V_{C2}}{V_0}, \quad z = \frac{\varphi}{\rho C_2 V_0}, \quad \tau = \frac{t}{\rho C_2}. \tag{5}$$

Furthermore, Eq. (4) can be redescribed as follows:

$$\begin{cases} \dfrac{dx}{d\tau} = c\left[-az(x+\mu) + x - \dfrac{x^3}{3} + b(y-x)\right], \\ \dfrac{dy}{d\tau} = u_s - dy - b(y-x), \\ \dfrac{dz}{d\tau} = -ez + \delta(x+\mu). \end{cases} \tag{6}$$

Here, x, y, and z are the state variables of the proposed neuron model. Specifically, (x, y) denote the membrane variables of the neuron and characterize its firing activity. z corresponds to the memristive state variable describing the ion channel of the neuron. The parameters in Eq. (6) are defined by

$$\begin{aligned} &u_s = \frac{\rho V_s}{V_0 R_s}, \quad a = \alpha\rho^2 C_2 V_0, \quad b = \frac{\rho}{R}, \\ &c = \frac{C_2}{C_1}, \quad d = \frac{\rho}{R_s}, \quad e = \lambda\rho C_2, \quad \mu = \frac{E}{V_0}. \end{aligned} \tag{7}$$

The physical field energies of the three energy storage components in the neural circuit are estimated as follows:

$$W = 0.5C_1V_{C1}^2 + 0.5C_2V_{C2}^2 + 0.5\varphi i_M. \tag{8}$$

Moreover, the Hamilton energy of the physical field energies is approximated by

$$H = \frac{W}{C_2 V_{C2}^2} = \frac{1}{2c}x^2 + \frac{1}{2}y^2 + \frac{1}{2}az^2(x+\mu). \tag{9}$$

From Eq. (9), the Hamilton energies depend on parameters (a, c, μ) and variables (x, y, z). In fact, the Hamilton energy is also calculated by using Helmholtz's law. First, the dynamic equations in Eq. (6) can be expressed as follows:

$$\begin{aligned}
\begin{pmatrix} \dot{x} \\ \dot{y} \\ \dot{z} \end{pmatrix} &= \begin{pmatrix} c[b(y-x) - (1/3)x^3 - az(x+\mu) + x] \\ u_s - b(y-x) - dy \\ -ez + \delta(x+\mu) \end{pmatrix} = F_c + F_d \\
&= \begin{pmatrix} y \\ -(1/c)x - 0.5az^2 \\ 0 \end{pmatrix} + \begin{pmatrix} c[-az(x+\mu) + x - (1/3)x^3 + b(y-x) - (1/c)y] \\ u_s - b(y-x) + 0.5az^2 - dy + (1/c)x \\ -ez + \delta(x+\mu) \end{pmatrix} \\
&= \begin{pmatrix} 0 & 1 & 0 \\ -1 & 0 & 0 \\ 0 & 0 & 0 \end{pmatrix} \begin{pmatrix} (1/c)x + 0.5az^2 \\ y \\ az(x+\mu) \end{pmatrix} + \begin{pmatrix} A_{11} & 0 & 0 \\ 0 & A_{22} & 0 \\ 0 & 0 & A_{33} \end{pmatrix} \begin{pmatrix} (1/c)x + 0.5az^2 \\ y \\ az(x+\mu) \end{pmatrix}, \\
A_{11} &= \frac{c[-az(x+\mu) + x - (1/3)x^3 + b(y-x) - (1/c)y]}{(1/c)x + 0.5az^2}, \\
A_{22} &= \frac{u_s - b(y-x) + 0.5az^2 - dy + (1/c)x}{y}, \quad A_{33} = \frac{-ez + \delta(x+\mu)}{az(x+\mu)}.
\end{aligned} \tag{10}$$

Here, $F_c(*)$ denotes the gradient field, and $F_d(*)$ is the vorticity field. The conditions they meet are

$$\nabla H^T F_c(X) = 0, \quad \dot{H} = \frac{dH}{d\tau} = \nabla H^T F_d(X). \tag{11}$$

As a result, Eq. (9) follows from solving the following equation:

$$y\frac{\partial H}{\partial x} - ((1/c)x + 0.5az^2)\frac{\partial H}{\partial y} + 0 \cdot \frac{\partial H}{\partial z} = 0. \tag{12}$$

Furthermore, we design a parameter adaptive growth scheme with energy proportion control to explore the self-regulating characteristics of biological neural functions, and the scheme is defined as follows:

$$\frac{dc}{d\tau} = \sigma \cdot c \cdot \vartheta\left(\varepsilon - \left|\frac{H_{c1}}{H}\right|\right), \tag{13}$$

where ε is an energy threshold and σ denotes the parameter growth gain. In principle, other parameters can also serve as the target of adaptive control, such as a and d.

3. Numerical simulation results

From the viewpoint of neurodynamics, the firing characteristics of a neuron can be controlled by different intensities of external stimuli. In this work, for simplicity, a periodic external stimulus signal is used to investigate the firing behavior of the dual-capacitor memristor neuron without an inductor. Here, the periodic external stimulus is selected as $u_s = A_1 \cos(f\tau)$; parameters of Eq. (6) are $a = 1.5$, $b = 0.5$, $c = 13.8$, $d = 3$, $e = 0.2$, $\delta = 0.15$, $f = 2.75$, $\mu = 1$, and the initial value is (0.1, 0.1, 0.1). Using the ode45 algorithm in MATLAB software, the solution to the differential equation in Eq. (6) is obtained. Furthermore, the evolution of the peak of the membrane variable x by changing A_1 and the corresponding largest Lyapunov exponent (LLE) of Eq. (6) are calculated in Fig. 2.

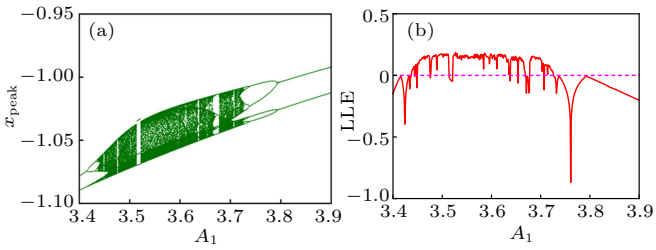


Fig. 2. The peak varying with A_1 and LLE. (a) Peak of membrane variable x; (b) LLE of neuron model presented in Eq. (6).

The results shown in Fig. 2 indicate that as the A_1 of the external stimulus continuously increases, the chaotic electrical activity behavior of the neurons will be suppressed, and the neurons will exhibit highly ordered periodic electrical activity behavior. During this period, neurons also exhibit significant chaotic and periodic alternation windows. Under chaotic behavior, the LLE of the model equation is greater than zero, while the LLE of the periodic state is less than zero. Moreover, the LLE of the model at the periodic bifurcation point is 0.

To observe the firing behaviors of neurons in response to external stimuli of varying intensities more clearly, Fig. 3 plots the time series of the membrane variable x and the corresponding energy series under different external stimulus intensities A_1, while maintaining the parameters and initial values described above.

Figure 3 clearly shows that when the periodic external stimulus $A_1 = 3.629$, the neuron exhibits chaotic electrical activity. However, when the periodic external stimulus $A_1 = 3.9$,

the neuron exhibits a two-cycle firing pattern. Furthermore, when the neuron exhibits chaotic electrical activity, the neuronal model has a lower $\langle H \rangle$, whereas during periodic firing, the neuron has a higher $\langle H \rangle$. In addition, Fig. 4 plots the trajectories of the neurons in the x–z plane corresponding to the electrical activity shown in Fig. 4.

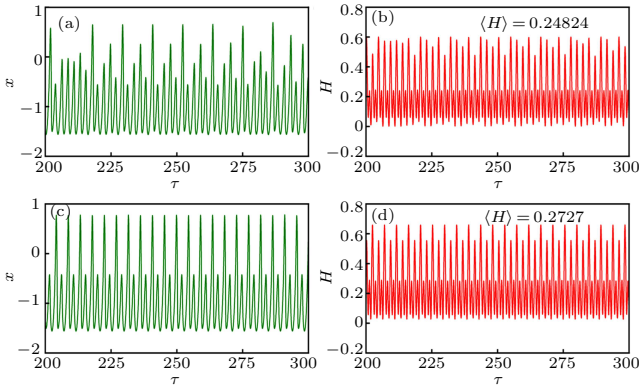


Fig. 3. The time-series of variable x and the corresponding energy series under different values of A_1: (a), (b) $A_1 = 3.629$; (c), (d) $A_1 = 3.9$. $\langle H \rangle$ is the energy average value within 100 units of time.

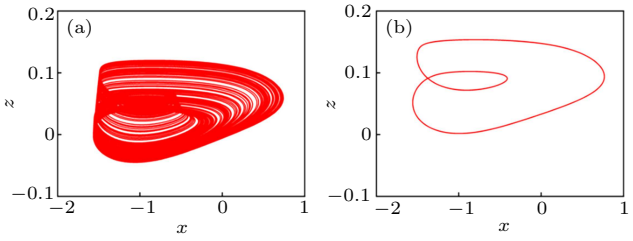


Fig. 4. Attractor diagrams of the x–z plane for different values of A_1: (a) $A_1 = 3.629$ (chaotic), (b) $A_1 = 3.9$ (periodic).

As shown in Fig. 4, as the trajectories of the neural system evolve in phase space, they are confined within a bounded region and do not exhibit a tendency to diverge to infinity. This indicates that the system is dissipative or stable on a long-term timescale. In Fig. 4(b), the trajectories form a closed, smooth curve, indicating that the system enters a state of periodic oscillation with a single dominant frequency and its harmonics.

The numerical simulation results presented above investigate the effect of the amplitude of periodic external stimuli on the electrical activity characteristics of neurons. Furthermore, the effect of the frequency of periodic external stimuli on neuronal electrical activity is examined. With the parameters and initial values maintained as above and the amplitude set to $A = 3.6$, the evolution of the peak of membrane variable x by changing f and the corresponding LLE of Eq. (6) is calculated in Fig. 5.

Figure 5 shows that the periodic electrical activity of neurons gives rise to chaotic electrical activity by increasing the frequency of the periodic external stimulus. Moreover, neurons also exhibited significant chaotic and periodic alternation windows in this period. The LLE of the model equation is greater than zero during chaotic behaviors, while the LLE of the periodic state is less than zero, and the LLE of the model at the periodic bifurcation point is 0.

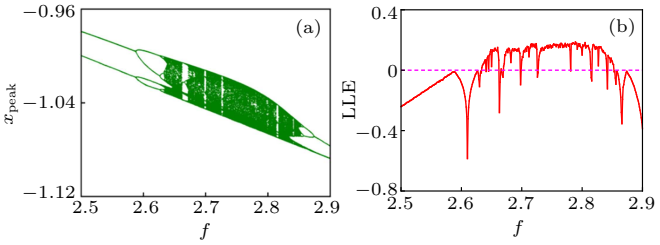


Fig. 5. The peak varying with f and LLE. (a) Peak of membrane variable x; (b) LLE of neuron model presented in Eq. (6).

To more clearly observe the electrical activity of neurons in response to the frequency of periodic external stimuli of varying intensities, Fig. 6 plots the time series of the membrane variable x and the corresponding energy series for different external stimulus intensities f, while maintaining the parameters and initial values described above.

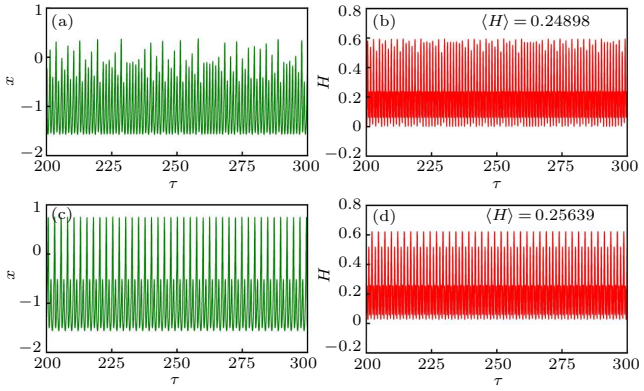


Fig. 6. The time-series of membrane variable x and the corresponding energy series with different values of f: (a), (b) $f = 2.77$; (c), (d) $f = 2.54$. $\langle H \rangle$ is the energy average value within 100 units of time.

Similarly, when the periodic external stimulus is $f = 2.77$, the neuron exhibits chaotic electrical activity. However, when the periodic external stimulus is $f = 2.54$, the neuron exhibits a two-cycle firing pattern. Furthermore, when the neuron exhibits chaotic electrical activity, the neuronal model has a lower $\langle H \rangle$, whereas during periodic firing, the neuron has a higher $\langle H \rangle$. In addition, Fig. 7 plots the trajectories of the neurons in the x–z plane corresponding to the electrical activity shown in Fig. 6.

From Fig. 7, as the trajectories of the neural system evolve in phase space, they are confined within a bounded region and do not exhibit a tendency to diverge to infinity. This indicates that the system is dissipative or stable on a long-term timescale. In Fig. 7(b), the trajectories form a closed, smooth curve, indicating that the system enters a state of periodic oscillation with a single dominant frequency and its harmonics.

Neurons are considered as electrically charged entities, and they are susceptible to the influence of external electromagnetic fields. Since magnetically controlled memristors can capture the external magnetic field, the impact of such fields on the firing behaviors of neurons is investigated in greater detail. First, the effects of a constant magnetic field on the electrical

activity of neurons are investigated. The parameters and initial values are maintained as above, and the periodic external stimulus is fixed to $u_s = 3.6\cos(2.75\tau)$; a constant magnetic field M_1 is added into the third equation of Eq. (6). Similarly, the evolution of the peak of the membrane variable x by changing M_1 and the corresponding LLE of Eq. (6) is plotted in Fig. 8.

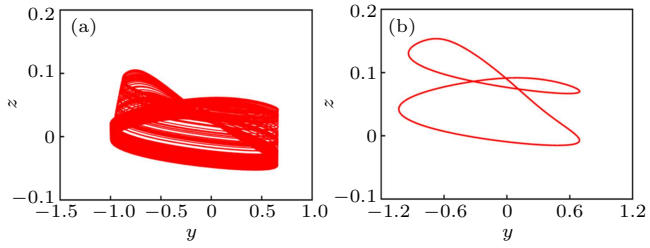


Fig. 7. Attractor diagrams of the y–z plane for different values of f: (a) $f = 2.77$ (chaotic), (b) $f = 2.54$ (periodic).

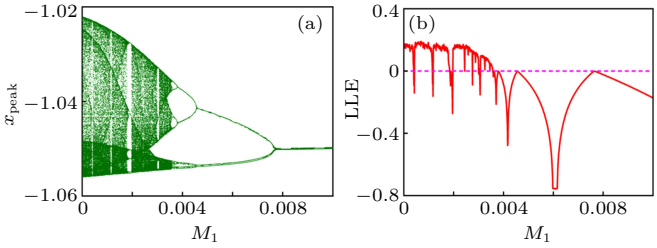


Fig. 8. The peak varying with M_1 and LLE. (a) Peak of membrane variable x; (b) LLE of the neuron model presented in Eq. (6).

The results shown in Fig. 8 indicate that as the intensity of the external magnetic field continuously increases, the chaotic electrical activity behavior of the neurons will be suppressed, and the neurons will exhibit highly ordered periodic electrical activity behavior. During this period, neurons also exhibited significant chaotic and periodic alternation windows. Under chaotic behavior, the LLE of the model equation is greater than zero, while the LLE of the periodic state is less than zero. Moreover, the LLE of the model at the periodic bifurcation point is 0. Similarly, Fig. 9 plots the time series of the membrane variable x and the corresponding energy series for different external magnetic intensities M_1, while maintaining the parameter and initial values described above.

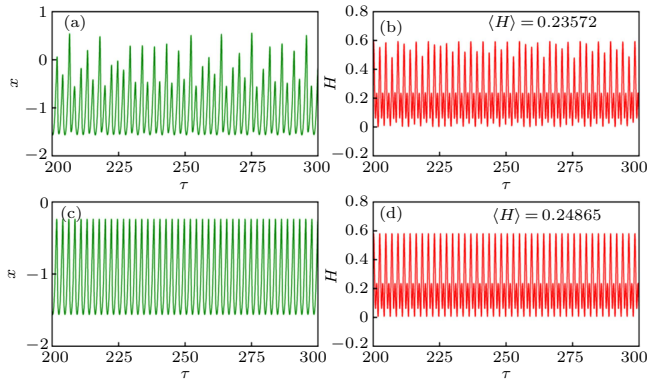


Fig. 9. The time-series of variable x and the corresponding energy series under different values of M_1: (a), (b) $M_1 = 0.001$; (c), (d) $M_1 = 0.01$. $\langle H\rangle$ is the energy average value within 100 units of time.

Similarly, when the constant magnetic field is $M_1 = 0.001$, the neuron exhibits chaotic electrical activity. However, when the constant magnetic field is $M_1 = 0.01$, the neuron exhibits a two-cycle firing pattern. Furthermore, when the neuron exhibits chaotic electrical activity, the neuronal model has a lower $\langle H\rangle$, whereas during periodic firing, the neuron has a higher $\langle H\rangle$. In addition, a periodic magnetic field $A_2\cos(2.75\tau)$ is added to the third equation of Eq. (6). Similarly, the evolution of the peak of the membrane variable x with changing A_2, and the corresponding LLE of Eq. (6), is plotted in Fig. 10.

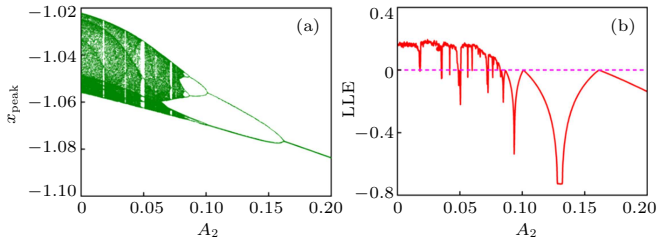


Fig. 10. The peak varying with A_2 and LLE. (a) Peak of membrane variable x; (b) LLE of the neuron model presented in Eq. (6).

Figure 10 indicates that the electrical activity of neurons can be modulated by adjusting the amplitude of an external periodic magnetic field. As the amplitude of the periodic external magnetic field increases, the periodic electrical activity of the neurons is induced to become chaotic. When the external magnetic field continues to increase, the chaotic electrical activity is suppressed, and the neurons exhibit periodic electrical activity. During this period, neurons also exhibit significant chaos and periodic alternating windows. Under chaotic behavior, the LLE of the model equation is greater than zero, while the LLE of the periodic state is less than zero. Moreover, the LLE of the model at the periodic bifurcation point is 0. Similarly, Fig. 11 plots the time series of membrane variable x and the corresponding energy series for different external magnetic intensities A_2, while maintaining the parameters and initial values described above.

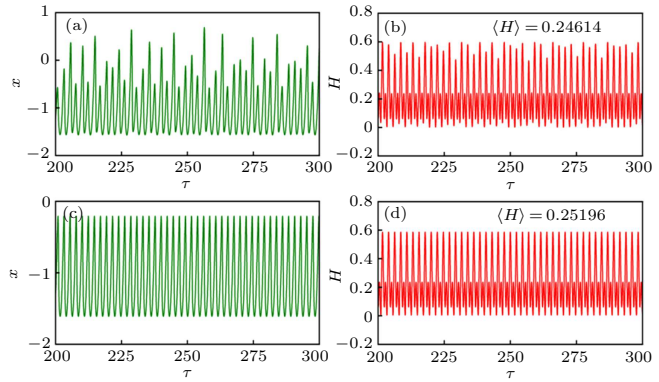


Fig. 11. The time-series of variable x and the corresponding energy series with different values of A_2: (a), (b) $A_2 = 0.025$; (c), (d) $A_2 = 0.17$. $\langle H\rangle$ is the energy average value within 100 units of time.

Similarly, when $A_2 = 0.025$, the neuron exhibits chaotic electrical activity. However, when $A_2 = 0.17$, the neuron exhibits a two-cycle firing pattern. Furthermore, when the neuron exhibits chaotic electrical activity, the neuronal model has a lower $\langle H \rangle$, whereas during periodic firing the neuron has a higher $\langle H \rangle$. In addition, Fig. 12 plots the trajectories of the neurons in the x–y plane corresponding to the electrical activity shown in Fig. 11.

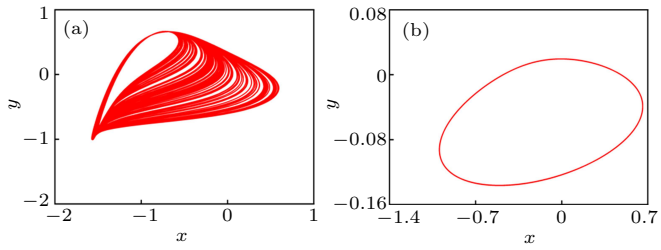


Fig. 12. Attractor diagrams of the x–y plane for different values of A_2: (a) $A_2 = 0.025$ (chaotic), (b) $A_2 = 0.17$ (periodic).

From Fig. 12, as the trajectories of the neural system evolve in phase space, they are confined within a bounded region and do not exhibit a tendency to diverge to infinity. This indicates that the system is dissipative or stable on a long-term timescale. In Fig. 12(b), the trajectories form a closed, smooth curve, indicating that the system enters a state of periodic oscillation with a single dominant frequency and its harmonics.

From the viewpoint of nonlinear dynamics, a nonlinear system subjected to the combined influence of an external periodic signal and noise can exhibit the phenomenon of stochastic resonance. To explore the phenomenon of stochastic resonance in the neuron model in Eq. (6), the parameters are fixed as $a = 1.5$, $b = 0.5$, $c = 13.8$, $d = 3$, $e = 0.2$, $\delta = 0.15$, $\mu = 1$, $u_s = 3.6\cos(2.75\tau)$, and the initial condition is (0.1, 0.1, 0.1). The third term in the neuronal model is expressed in Eq. (6), where an external Gaussian white noise magnetic field is applied. Then, the evolution of the signal-to-noise ratio (SNR) and energy average value $\langle H \rangle$ with varying noise intensity D is shown in Fig. 13.

Figure 13 shows that when the intensity of the Gaussian white noise magnetic field is 0.453, both the SNR and $\langle H \rangle$ reach values of 0.979 and 0.225, respectively. This indicates the occurrence of stochastic resonance in the neuronal dynamical model, which signifies a high degree of order in the oscillations of the neuronal model. Furthermore, the self-regulatory properties of neurons were investigated using the neuronal model described by Eq. (6) and the parameter-adaptive growth method described by Eq. (13). The parameters and initial values in Eq. (6) remain as above; the energy ratio threshold in Eq. (13) is $\varepsilon = 0.6$, and the initial value of the parameter is $c = 13.8$. Figure 14 plots the evolution of the parameters over time and the evolution of the membrane variable sequence for different gains.

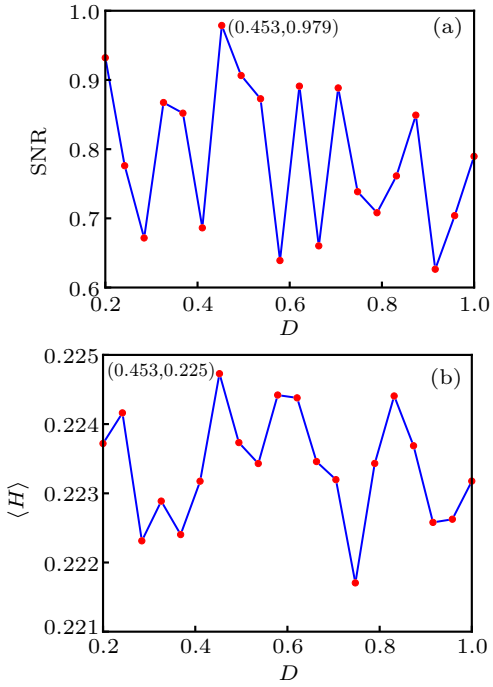


Fig. 13. (a) SNR with varying D; (b) $\langle H \rangle$ with varying D.

It can be seen from Fig. 14 that the parameter c reaches a stable threshold after a certain time interval, and the sequence of membrane variables also transitions from a chaotic pattern to an ordered periodic pattern. This demonstrates that the designed adaptive regulation method is capable of adaptively regulating chaotic neurons into a periodic oscillatory pattern. Furthermore, chaotic neurons can rapidly enter a periodic pattern by increasing the gain.

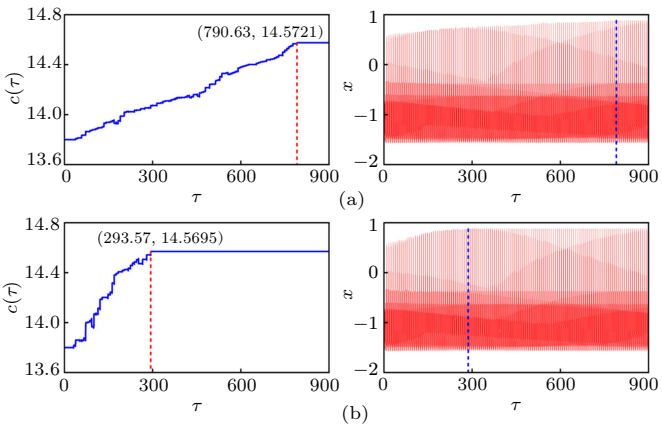


Fig. 14. The evolution of parameters c and x for different gain values σ: (a) $\sigma = 0.02$, (b) $\sigma = 0.05$.

To investigate the dynamical behaviors of neurons, when the other parameters and initial values in Eq. (6) remain as above, the SE complexity under different values of system parameters is plotted in Fig. 15.

The result in Fig. 15 shows that the chaotic state has a higher complexity value, and the periodic pattern has a lower complexity value. To verify the validity of the hardware implementation of the neuron model in Eq. (6), the neuron model in Eq. (6) can be updated as follows:

$$\begin{cases} C_1\dfrac{\mathrm{d}V_1}{\mathrm{d}t} = \dfrac{R_{12}}{R_{21}R_1}V_1 + \dfrac{R_{12}}{R_{21}R_2}V_1^3 + \dfrac{R_{12}}{R_{21}R_3}V_1V_3 + \dfrac{R_{12}}{R_{21}R_4}V_3 + \dfrac{R_{12}}{R_{21}R_5}V_2, \\ C_2\dfrac{\mathrm{d}V_2}{\mathrm{d}t} = \dfrac{R_{13}}{R_{22}R_6}V_1 + \dfrac{R_{13}}{R_{22}R_7}S_2 + \dfrac{R_{13}}{R_{22}R_8}V_2, \\ C_3\dfrac{\mathrm{d}V_3}{\mathrm{d}t} = \dfrac{R_{14}}{R_{23}R_9}V_1 + \dfrac{R_{14}}{R_{23}R_{10}}V_3 + \dfrac{R_{14}}{R_{23}R_{11}}S_1. \end{cases} \tag{14}$$

The equivalent circuit corresponding to Eq. (14) is shown in Fig. 16.

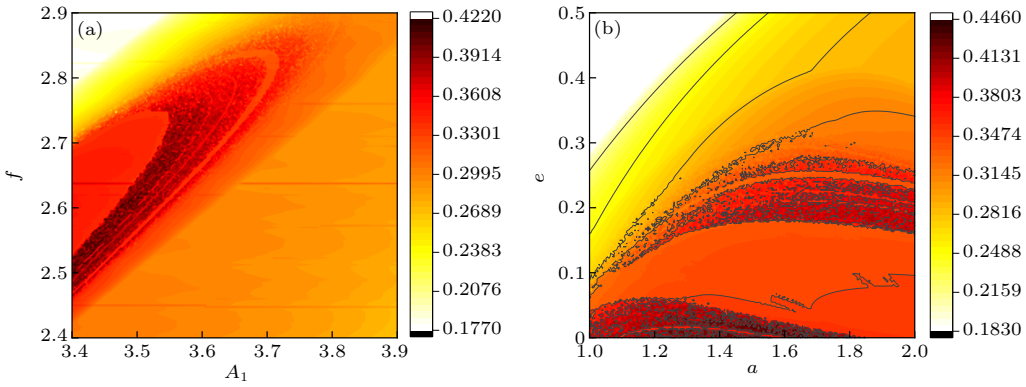


Fig. 15. (a) *SE* complexity diagram under different A_1 and f. (b) *SE* complexity diagram under different a and e.

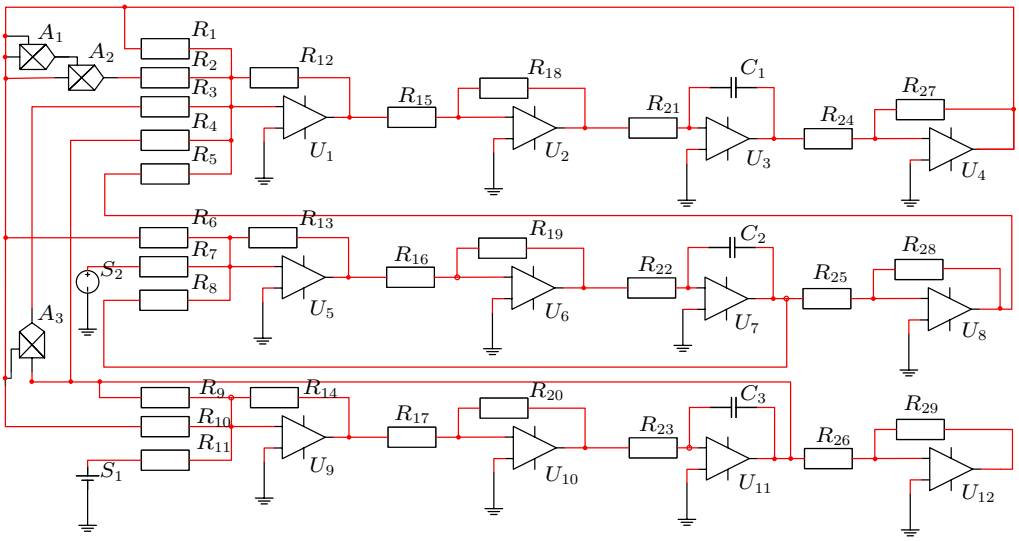


Fig. 16. The equivalent circuit corresponding to Eq. (14).

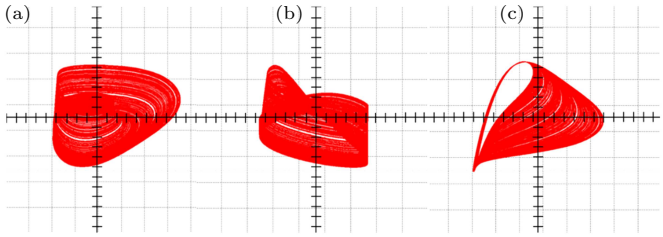


Fig. 17. The LTspice simulation results. (a) Attractor diagrams of the x–z plane; (b) attractor diagrams of the y–z plane, (c) attractor diagrams of the x–y plane.

Here, when $S_1 = 1$ V, $S_2 = 3.629\cos(4.379t)$ V, $R_i = 100$ kΩ ($i = 15, 16, 17, 18, 19, 20, 24, 25, 26, 27, 28, 29$), $R_j = 1$ MΩ ($j = 12, 13, 14, 21, 22, 23$), $R_1 = R_5 = 144.93$ kΩ, $R_2 = 217.4$ kΩ, $R_3 = R_4 = 48.3$ kΩ, $R_6 = 2$ MΩ, $R_7 = 1$ MΩ, $R_8 = 286$ kΩ, $R_9 = 5$ MΩ, $R_{10} = R_{11} = 6.67$ MΩ, $C_1 = C_2 = C_3 = 1$ nF, the LTspice simulation results are shown in Fig. 17.

The results shown in Fig. 17 are consistent with the previous numerical simulation results, indicating that this neuronal model can be effectively implemented in a physical circuit.

4. Conclusions

This paper designs a dual-capacitor memristive neuron circuit without any inductive elements, and then a neuron dynamic model expressed by a differential equation is derived by applying Kirchhoff's current law and using the Helmholtz theorem to verify the energy function. The nonlinear dynamics of the neuron model are researched using nonlinear dynamic analysis methods. The results show that the periodic electrical activity of neurons gives rise to chaotic electrical activity by increasing the frequency of the external stimulus. The elec-

trical activity of neurons can be modulated by changing the intensity or amplitude of the magnetic field. When the neuron exhibits chaotic electrical activity, the neuronal model has a lower average energy value, whereas during periodic firing, the neuron has a higher average energy value. The random resonance phenomenon can also occur under a noisy magnetic field. The self-regulation of the neuron is simulated by an adaptive method of energy ratio control. The LTspice simulation is further employed to verify the hardware implementation of the neuron model. This neuron model can be coupled to form a neuronal network, enabling the investigation of the collective behaviors of neuronal networks and the influence of external magnetic fields on their collective properties. Future work will focus on the hardware implementation and large-scale integration of memristive neural networks based on the proposed inductor-free neuron circuit, while extending the framework to magnetic-controlled memristors to investigate richer electromagnetic coupling dynamics.

Acknowledgement

This work is completed with the support of the National Natural Science Foundation of China (Grant No. 62273272).

References

[1] Chua L 2003 *IEEE Transactions on Circuit Theory* **18** 507
[2] Strukov D, Snider G, Stewart D and Williams R 2008 *Nature* **453** 80
[3] Bao B, Ma Z, Xu J, Liu Z and Xu Q 2011 *International Journal of Bifurcation and Chaos* **21** 2629
[4] Wu R and Wang C 2016 *International Journal of Bifurcation and Chaos* **26** 1650145
[5] Xujiong M, Mou J, Liu J, Ma C, Yang F and Zhao X 2020 *Nonlinear Dyn.* **100** 2859
[6] Jiang C, Liu Y, Zhang F, Gu X, Zhang M and Zhao Y 2025 *Physica Scripta* **100** 125212
[7] Khan N A, Qureshi M A, Akbar S and Ara A 2022 *Physica Scripta* **98** 014002
[8] Wu S, Rong X and Liu Z 2019 *Journal of System Simulation* **30** 3985
[9] Rajagopal K, Kacar S, Wei Z, Duraisamy P, Kifle T and Karthikeyan A 2019 *AEU-International Journal of Electronics and Communications* **107** 183
[10] Bao B C, Bao H, Wang N, Chen M and Xu Q 2017 *Chaos, Solitons & Fractals* **94** 102
[11] Li Y, Wang M, Chang H, Wang H and Chen G R 2024 *Nonlinear Dyn.* **112** 3851
[12] Prousalis D A, Volos C K, Stouboulos I N and Kyprianidis M I 2017 *Nonlinear Dyn.* **90** 1681
[13] Saha P, Saha D C, Ray A and Chowdhury A R 2015 *Euro. Phys. J. Spec. Top.* **224** 1563
[14] Wang X, Gao M, Iu H H C and Wang C H 2022 *Chaos, Solitons & Fractals* **159** 112177
[15] Yu F, Zhang W, Xiao X, Yao W, Cai S, Zhang J, Wang C and Li Y 2024 *Fractal and Fractional* **8** 271
[16] Zhao B, Xu S and Wang G 2024 *Physica Scripta* **99** 125203
[17] Wang M, Deng Y, Liao X, Li Z, Ma M and Zeng Y 2019 *International Journal of Non-Linear Mechanics* **111** 149
[18] Yan S, Ren Y, Song Z, Shi W and Sun X 2022 *Integration* **85** 63
[19] Xiu C, Fang J and Ma X 2022 *Chaos, Solitons & Fractals* **161** 112409
[20] Tayyab M, Sun K, Yao Z and Wang H 2024 *Physica Scripta* **99** 085273
[21] Guo Z, Wen J and Mou J 2022 *Mathematics* **11** 24
[22] Dong C and Yang M 2024 *Chinese Journal of Physics* **89** 930
[23] Liu X, Sun K, Wang H and He S 2023 *Chaos, Solitons & Fractals* **174** 113791
[24] Li Y, Li C, Zhong Q, Liu S and Lei T 2024 *Nonlinear Dyn.* **112** 3869
[25] Han X, Mou J, Lu J, Lu J, Banerjee S and Cao Y 2023 *Fractals* **31** 2340104
[26] Wang Y, Song X L and Yang F 2025 *Chin. Phys. B* **34** 090504
[27] Yu Z, He J, Song X and Yang F F 2025 *Euro. Phys. J. Plus* **140** 405
[28] Yang F, Ren L, Ma J and Zhu Z 2024 *Journal of Zhejiang University-Science A* **25** 382
[29] Yang F, He J, Song X, Yin H and Chen J 2026 *AEU-International Journal of Electronics and Communications* **206** 156195
[30] Yang F, Song X, He J and Yin H 2026 *Journal of Zhejiang University-SCIENCE A* **27** 76
[31] Baysal V, Solmaz R and Ma J 2023 *Applied Mathematics and Computation* **448** 127940
[32] Calim A and Baysal V 2023 *Chaos, Solitons Fractals* **176** 114105
[33] Baysal V, Saraç Z and Yilmaz E 2019 *Nonlinear Dyn.* **97** 1275
[34] Tan Y and Wang C 2020 *Chaos* **30** 053118
[35] Alexander P, Natiq H, Ghasemi M, Karthikeyan A, Jafari S and Rajagopal K 2024 *Euro. Phys. J. Plus* **139** 133
[36] Gao Y, Li C, Cen X, Zhang X and Xu J 2025 *Chin. J. Phys.* **95** 1185
[37] Amiri F G, Nazarimehr F, Jafari S and Towhidkhah F 2024 *Chin. J. Phys.* **89** 1400
[38] Xie Y, Ye Z, Li X, Wang X and Jia Y 2024 *Cognitive Neurodynamics* **18** 1989
[39] Lei Z, Guo Q, Wang C and Ma J 2025 *Journal of Zhejiang University-Science A* **26** 755
[40] Yang F, Xu Y and Ma J 2023 *Chaos* **33** 023110
[41] Yang F, Ren G and Tang J 2023 *Nonlinear Dyn.* **111** 21917
[42] Song X and Yang F 2025 *Journal of Theoretical Biology* **599** 112034
[43] Guo Y, Wu F, Yang F and Ma J 2023 *Chaos* **33** 113106
[44] Yang F, Song X and Yu Z 2024 *Chaos, Solitons & Fractals* **188** 115496
[45] Wan J, Wu F, Ma J and Wang W 2024 *Chin. Phys. B* **33** 050504
[46] Yang F, Song X and Yu Z 2025 *Nonlinear Dyn.* **113** 7213
[47] Yu Z, Zhu K, Wang Y and Yang F 2025 *Chaos, Solitons & Fractals* **194** 116233
[48] Yang F, Song X and Xu Y 2025 *Chaos, Solitons & Fractals* **199** 116740
[49] Wang C, Lv M, Alsaedi A and Ma J 2017 *Chaos. Nov.* **27** 113108
[50] Xu Q, Liu T, Ding S K, Bao H, Li Z and Chen B 2023 *Cognitive Neurodynamics* **17** 755
[51] Bao H, Li K X, Ma J, Hua Z Y, Xu Q, Bao B C Science 2023 *Science China Technological Sciences* **66** 3153
[52] Feng X S, Wu F Q and Ma J 2025 *Science China Technological Sciences* **68** 2120402